Frequency- and Time-Domain Analyses of Nonuniform Lossy Coupled Transmission Lines with Linear and Nonlinear Terminations

Noureddine Boulejfen, Ammar B. Kouki, *Member, IEEE*, and Fadhel M. Ghannouchi, *Senior Member, IEEE*

***Abstract*—A new technique for the frequency- and time-domain characterization of nonuniform coupled transmission lines is presented in this paper. In the frequency domain, a method-of-moments-based approach is used to compute the $2N \times 2N$ scattering parameter matrix of the N-coupled lines using special frequency-dependent basis functions that give good accuracy over very large bandwidths. In the time domain, the structure's S-parameters are used as its Green's function and are combined with source and terminating load conditions to obtain its transient response. The proposed method can account for loss and is particularly suitable for wide-band microwave component designs and ultrahigh-speed/large-bandwidth digital interconnects, including nonlinear terminating loads. A detailed formulation of both the frequency- and time-domain approaches is presented. Several examples of two- and three-line structures are analyzed and the results are compared to published results and other computer-aided-design simulations.**

***Index Terms*—Coupled lines, nonuniform lines, transient analysis, transmission lines.**

I. Introduction

TODAY'S technological trend towards higher performing microwave and digital circuits at increasingly smaller sizes poses new challenges to both the microwave and high-speed VLSI designers. One aspect of these challenges lies in the fact that nonuniform transmission structures must often be used to reduce circuit sizes, to increase circuit bandwidth, to reduce discontinuity effects, and to optimize the overall circuit performance. While several alternative techniques are available for modeling and analyzing single nonuniform lines, the same cannot be said of multiple coupled lines where significantly less work has been carried out and where no computer-aided-design (CAD) suitable methods are currently available. In fact, aside from [1], where several piecewise uniform multiconductor transmission-line segments have been cascaded, or [2] and [3], where a moment-method approach with spatially fixed basis functions has been suggested, little other literature is available on the subject. Moreover, both of these approaches have limitations that make them impractical CAD tools, particularly when analyzing a large number of lines and at high frequencies. This latter problem is of particular interest to high-speed digital-circuit designers who deal with very short fast-rising pulses, i.e., wide-band frequency content, in multiconductor interconnects.

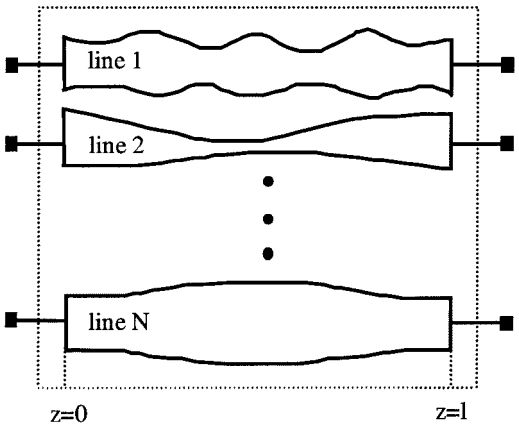

Fig. 1. N-coupled nonuniform transmission lines.

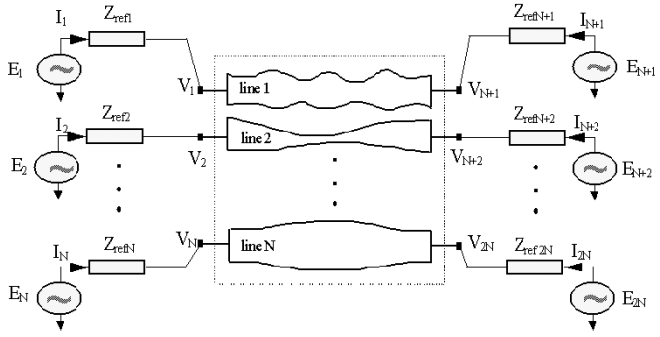

(a)

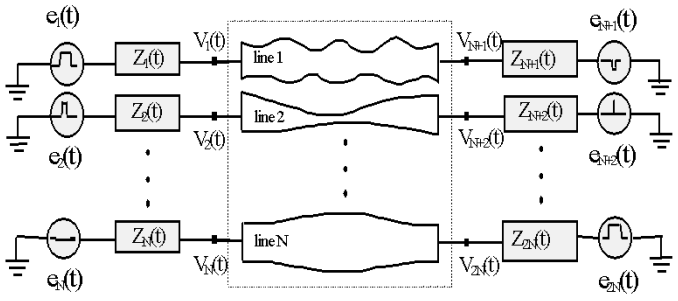

(b)

Fig. 2. Circuits for: (a) S-parameter calculation and (b) transient response with arbitrary loads calculation of a multiport network.

Manuscript received September 23, 1998; revised December 10, 1999.

N. Boulejfen and F. M. Ghannouchi are with Ecole Polytechnique de Montréal, Montréal, P.Q., Canada H3V 1A2.

A. B. Kouki is with Ecole de Technologie Superieure, Montréal, P.Q., Canada H3C 1K3.

Publisher Item Identifier S 0018-9480(00)02055-X.

In this paper, two new efficient and robust approaches for the frequency and transient analysis of multiple-coupled nonuniform transmission lines are proposed. In the frequency domain, a method-of-moments approach is used to compute the scattering parameters of the nonuniform structure under an arbitrary reference impedance system. This approach uses basis functions derived from the structure's own propagation characteristics; hence, building-in the proper frequency dependence. The accuracy of this technique is demonstrated by several examples and its efficiency is shown through an optimization of an ultrawide-band coupler design. In the time domain, the coupled nonuniform transmission lines are subject to arbitrary waveform excitations and linear or nonlinear terminating loads. For this analysis, the time-domain scattering parameters, obtained by a Fourier transform of the frequency-domain data, are used in a convolution algorithm to obtain the transient behavior of the structure. Since the frequency-domain S-parameters include loss, dispersion, and discontinuity effects, the transient response will also include these effects without any particular effort. Several examples are provided to validate the proposed approach, and the results are compared to those in the literature or obtained by commercial software packages.

II. Theory

Consider the section of N-coupled nonuniform transmission lines shown in Fig. 1. In general, this structure could represent part of a multiport microwave circuit or interconnection lines used in a high-speed digital circuit. Since it is a passive $2N$-port network, this structure is accurately and conveniently characterized by its frequency-domain S-parameters. Fig. 2(a) shows a typical setup for S-parameter calculation. Once the frequency-domain S-parameters are known, they can be transformed to the time domain and used to simulate the transient response of the structure, as shown in Fig. 2(b). The following sections detail the formulations used for both the frequency- and time-domain analyses of the nonuniform structure.

A. Frequency-Domain Analysis

Consider the section of N-coupled nonuniform transmission lines shown in Fig. 2(a). Such a structure is of interest in many microwave applications, such as couplers, filters, and matching circuits, where frequency bandwidth and smooth transitions are of particular importance. As a passive $2N$-port network, this structure is best characterized by its frequency-domain S-parameters. Considering quasi-TEM mode propagation, the distributions of the current and voltage waves in the coupled lines are governed by the well-known telegrapher's equations, which relate the individual line voltages $V_j(f, z)$ and currents $I_j(f, z)$ by

$$\frac{\partial I_j(f, z)}{\partial z} = -\sum_{k=1}^{N} Y^{jk}(f, z).V_k(f, z) \tag{1a}$$

$$\frac{\partial V_j(f, z)}{\partial z} = -\sum_{k=1}^{N} Z^{jk}(f, z).I_k(f, z) \tag{1b}$$

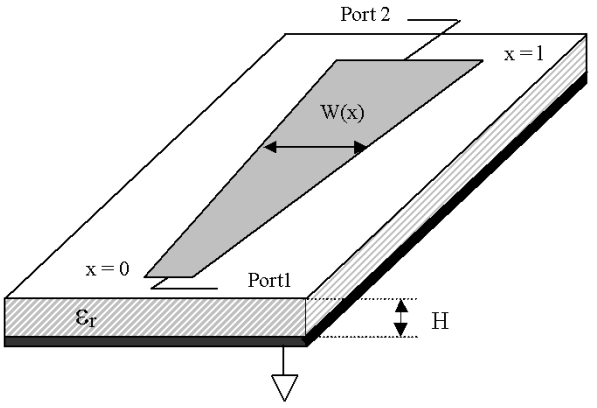

Fig. 3. Tapered microstrip line geometry: $W(0) = 10$ mil, $W(l) = 40$ mil, $\varepsilon_r = 9.9$, $H = 10$ mil, and $l = 5$ mm.

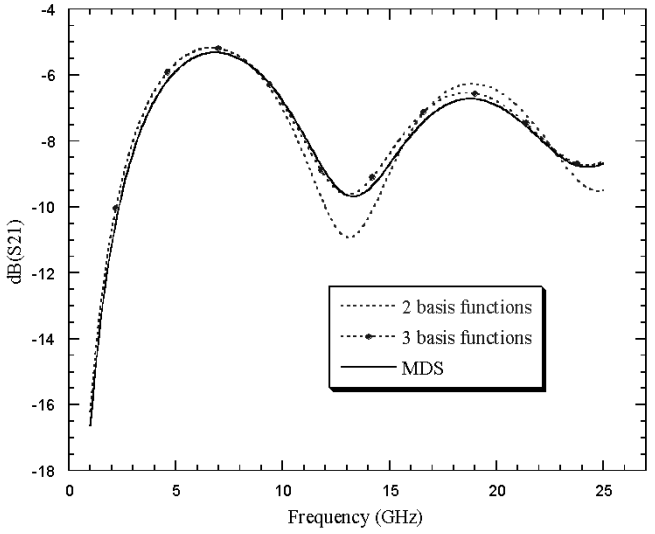

(a)

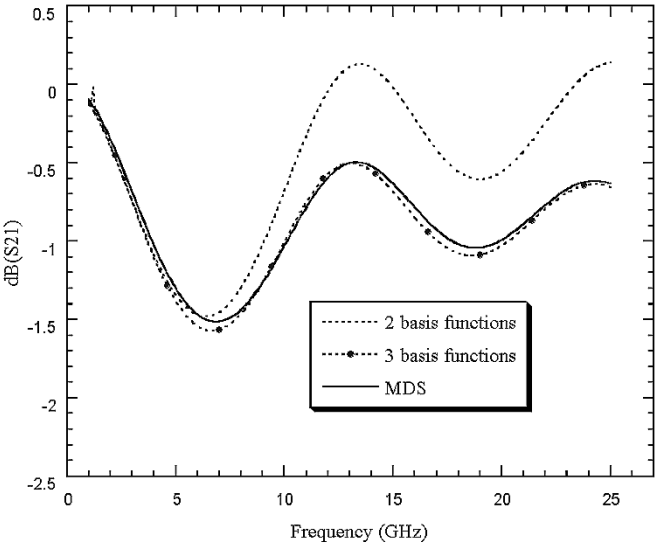

(b)

Fig. 4. Frequency-domain analysis of a linear microstrip taper. (a) Return loss. (b) Insertion loss.

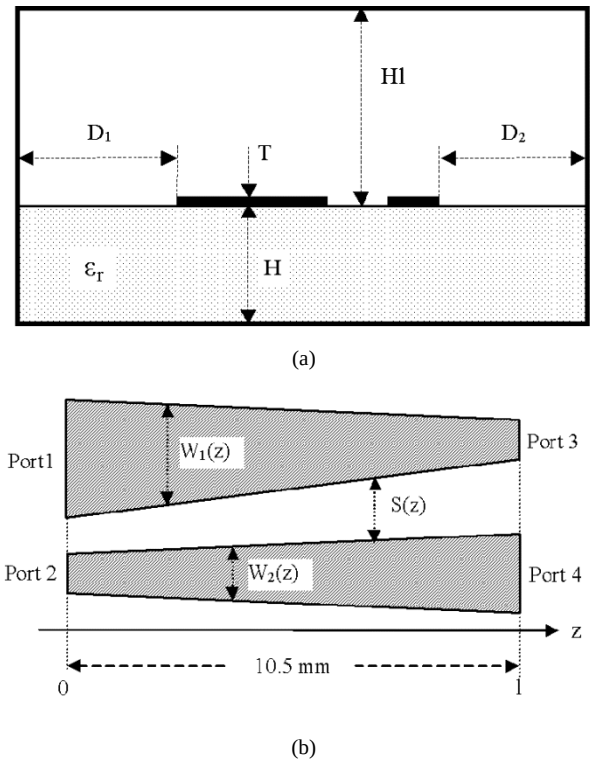

Fig. 5. Shielded asymmetric coupled microstrip lines. (a) Front view: $\varepsilon_r = 3.4$, $H = 10$ mil, $Hl = 50$ mil, $D_1 = D_2 = 1$ m, $T = 1$ μm, $\sigma = 10^7$ Ω^{-1}m, $\tan\delta = 0.001$. (b) Top view: $W_1(z) = 150(1 - 2z/3l)$ μm, $W_2(z) = S(z) = 50(1 + z/l)$ μm.

where f is the frequency, z is the direction of propagation, $Z^{jk}(f, z)$ and $Y^{jk}(f, z)$ are the entries of the frequency and position dependent per-unit length impedance and admittance matrices $Z(f, z)$, $Y(f, z)$. These entries are given in terms of the coupled lines' $RLGC$ matrices by $Z(f, z) = R(f, z) + j\omega L(f, z)$ and $Y(f, z) = G(f, z) + j\omega C(f, z)$ with $\omega = 2\pi f$. In general, these matrices are obtained by a two–dimensional (2-D) solution of Maxwell's equations at some positions along the propagation axis z. Depending on the nature and geometry of the structure being analyzed and the desired accuracy, one of several alternatives quasi-static or full-wave solution techniques may be used. These techniques will not be discussed in this paper and we will simply assume that these matrices are known at some discrete positions along the propagation axis z.

In previous works [2]–[5], (1a) and (1b), without any further manipulations, were solved by a method-of-moments approach, where both of the unknown current and voltage distributions on all lines were expanded in terms of a set of suitable basis functions. In [2] and [3], Chebyshev polynomials were used for this purpose, while in [4] and [5], a set of forward and backward propagating waves were used as the basis functions. The fact that both V and I are independently expanded in terms of basis functions introduces redundancy in the system since both quantities are already coupled through the telegrapher's equations. The redundancy thus introduced leads, as expected, and as shown in [6], to ill-conditioned matrices. Therefore, in order to make full use of the coupling between V and I in a method-of-moments formulation, (1a) and (1b) are manipulated as follows: first, multiplying (1b) by $Z^{-1}(f, z)$ and taking the derivative of the resulting expression with respect to z, the following equation is obtained:

$$Z^{-1}(f, z)\frac{\partial^2\overline{V}(f, z)}{\partial z^2} + \frac{\partial\left(Z^{-1}(f, z)\right)}{\partial z}\frac{\partial\overline{V}(f, z)}{\partial z} + \frac{\partial\overline{I}(f, z)}{\partial z} = \overline{0}_N \quad (2)$$

where the derivatives of the matrix and vector quantities are given by the derivatives of each of their entries. Next, expressing $\overline{I}(f, z)$ in terms of $\overline{V}(f, z)$ by using (1a), the following second-order differential equation for the complex voltage vector $\overline{V}$ can be obtained:

$$Z^{-1}\frac{\partial^2\overline{V}}{\partial z^2} + \frac{\partial Z^{-1}}{\partial z}\frac{\partial\overline{V}}{\partial z} - Y\overline{V} = \overline{0}_N \quad (3)$$

where Z, Y, and $\overline{V}$ are frequency- and z-dependent quantities. Note that an alternative option would be to use the identity that would yield to a differential equation of the form

$$\frac{\partial^2\overline{V}}{\partial z^2} - Z_pZ^{-1}\frac{\partial\overline{V}}{\partial z} - ZY\overline{V} = \overline{0}_N.$$

Equation (3) has been retained because it results in a computationally more efficient implementation. This equation can now be solved for the voltage distribution, from which the current distribution can be computed as per (1b). To perform this solution, a method-of-moments approach is used where only $\overline{V}(f, z)$ is expanded in terms of forward F_n and backward B_n propagating waves as follows:

$$\overline{V}(f, z) = \sum_{n=1}^{N_g}\overline{a}_nF_n(z, f) + \overline{b}_nB_n(z, f) \quad (4)$$

where a_n^j and b_n^j are the unknown coefficients associated with the nth basis function on the jth line, and N_g is the number of forward and backward waves used for the computation. The frequency-dependent basis functions are given by $F_n(z, f) = e^{-\gamma_n(f)z}$ and $B_n(z, f) = e^{\gamma_n(f)z}$, where $n = 1, \cdots, N_g$, and are defined over the entire domain $0 \le z \le l$. The set of γ_n values represents the propagation constants of the modes supported by the N-line structure computed at specified points z_i along the z-axis of propagation. They can be computed from the Z and Y matrices by [8]

$$\overline{\gamma}^2 = \mathrm{diag}(EZYE^{-1}) = \mathrm{diag}(HYZH^{-1}) \quad (5)$$

where E and H are the eigenvectors of the ZY and YZ matrix products, respectively. By computing the vector $\overline{\gamma}$ at an adequate number of points along the z-axis, and interpolating the resulting values, any desired number of basis functions can be formed.

Substituting (4) in (3) leads to the following equation:

$$\sum_{n=1}^{N_g}\left(Z^{-1}\gamma_n^2 - Z_p^{-1}\gamma_n - Y\right)\overline{a}_ne^{-\gamma_nz} + \left(Z^{-1}\gamma_n^2 + Z_p^{-1}\gamma_n - Y\right)\overline{b}_ne^{\gamma_nz} = \overline{0}_N \quad (6)$$

where $Z_p^{-1} = (\partial Z^{-1}(f, z)/\partial z)$. Testing (6) with $F_m(z, f)$ and $B_m(z, f)\,(m = 1, \cdots, N_g - 1)$ leads to a matrix equation whose entries are given in terms of the following inner products:

$$\begin{aligned} &\left\langle Z^{-1} e^{\pm\gamma_n z},\, e^{\pm\gamma_m z}\right\rangle \\ &\left\langle Z_p^{-1} e^{\pm\gamma_n z},\, e^{\pm\gamma_m z}\right\rangle \\ &\left\langle Y e^{\pm\gamma_n z},\, e^{\pm\gamma_m z}\right\rangle \end{aligned} \tag{7}$$

with the inner product being defined by

$$\langle f, g\rangle = \int_0^l f(z) g(z)\, dz \tag{8}$$

where l is the length of the structure. Using the above definition, the terms of (7) are easily calculated from knowledge of Z^{-1} and Y at discrete z-points with linear interpolation in between, i.e., $Z^{-1}(z) = A_z^i z + B_z^i$ and $Y(z) = A_y^i . z + B_y^i$ for $z_i \le z \le z_{i+1}$. With this interpolation, $Z_p^{-1}(z) = A_z^i$ and $Y_p(z) = A_y^i$ in the interval $[z_i,\, z_{i+1}]$. Finally, the matrix equation obtained after testing (6) can be written in two blocks as follows:

$$\sum_{n=1}^{N_g} \Big[K(m, n)\Big]\overline{a}_n + \Big[H(m, n)\Big]\overline{b}_n = \overline{0}_N \tag{9a}$$

$$\sum_{n=1}^{N_g} \Big[P(m, n)\Big]\overline{a}_n + \Big[Q(m, n)\Big]\overline{b}_n = \overline{0}_N \tag{9b}$$

where

$$\Big[K(m, n)\Big] = \sum_{i=1}^{N_s - 1} R_{0i, nm}^{--} T_{0i, n} + R_{1i, nm}^{--} T_{1i, n} \tag{10a}$$

$$\Big[H(m, n)\Big] = \sum_{i=1}^{N_s - 1} R_{0i, nm}^{+-} U_{0i, n} + R_{1i, nm}^{+-} T_{1i, n} \tag{10b}$$

$$\Big[P(m, n)\Big] = \sum_{i=1}^{N_s - 1} R_{0i, nm}^{-+} T_{0i, n} + R_{1i, nm}^{-+} T_{1i, n} \tag{10c}$$

$$\Big[Q(m, n)\Big] = \sum_{i=1}^{N_s - 1} R_{0i, nm}^{++} U_{0i, n} + R_{1i, nm}^{++} T_{1i, n} \tag{10d}$$

with

$$T_{0i, n} = \gamma_n^2 B_z^i - \gamma_n A_z^i - B_y^i \tag{11a}$$

$$U_{0i, n} = \gamma_n^2 B_z^i + \gamma_n A_z^i - B_y^i \tag{11b}$$

$$T_{1i, n} = \gamma_n^2 A_z^i - A_y^i \tag{11c}$$

and

$$R_{pi, nm}^{ab} = \int_{z_i}^{z_{i+1}} z^p e^{(a\gamma_n + b\gamma_m) z}\, dz, \qquad p = (0, 1);$$
$$a = (+, -); \quad b = (+, -). \tag{12}$$

Since there are $2N_gN$ unknowns and only $2(N_g - 1)N$ equations (9), additional $2N$ equations are needed to solve the system. These equations are derived from the additional boundary conditions imposed on structure. Let $Z_{\text{ref}}^0 = \text{diag}(Z_{\text{ref}}^1, Z_{\text{ref}}^2, \cdots, Z_{\text{ref}}^N)$ and $Z_{\text{ref}}^l = \text{diag}(Z_{\text{ref}}^{N+1}, Z_{\text{ref}}^{N+2}, \cdots, Z_{\text{ref}}^{2N})$ be the normalizing impedance matrices at $z = 0$ and $z = l$, respectively. To compute the scattering parameters, as shown in Fig. 2(a), the structure is excited by two voltage vectors $\overline{E}_0 = (E_1, E_2, \cdots, E_N)$ and $\overline{E}_l = (E_{N+1}, E_{N+2}, \cdots, E_{2N})$ through the Z_{ref}^0 and Z_{ref}^l port impedances, respectively. Thus, the equations obtained are

$$\overline{E}_0 = \overline{V}(f, 0) + Z_{\text{ref}}^0 \overline{I}(f, 0) \tag{13a}$$

$$\overline{E}_l = \overline{V}(f, l) - Z_{\text{ref}}^l \overline{I}(f, l). \tag{13b}$$

Using the expansion of $\overline{V}$ described in (4) and combining (13) with (1) leads to a set of $2N$ equations as follows:

$$\begin{aligned} \sum_{n=1}^{N_g} &\left(I_d + \gamma_n Z_{\text{ref}}^0 Z(f, 0)^{-1}\right)\overline{a}_n \\ &+ \left(I_d - \gamma_n Z_{\text{ref}}^0 Z(f, 0)^{-1}\right)\overline{b}_n = \overline{E}_0 \end{aligned} \tag{14a}$$

$$\begin{aligned} \sum_{n=1}^{N_g} &e^{-\gamma_n l}\left(I_d + \gamma_n Z_{\text{ref}}^l Z(f, l)^{-1}\right)\overline{a}_n \\ &+ e^{+\gamma_n l}\left(I_d - \gamma_n Z_{\text{ref}}^l Z(f, l)^{-1}\right)\overline{b}_n = \overline{E}_l. \end{aligned} \tag{14b}$$

By exciting only one port at a time, the system of $2N_gN$ linear equations given by (9) and (14) is solved for the voltage vector $\overline{V}(f, z)$. Once the voltage is known at all ports of the structure, the S-parameters can be extracted using the definition

$$S_{mn} = \frac{\left(1 + e^{-2j\theta_m}\right) V_{mn} - e^{-2j\theta_m} E_{mn}}{E_{nn}} \sqrt{\frac{R_n}{R_m}} \tag{15}$$

where θ_m is the angle of Z_{ref}^m, R_m is its real part, V_{mn} is the voltage at port m when the port n is excited, and E_{mn} is the excitation voltage used. $E_{mn} = 1$ when $m = n$ and zero when $m \ne n$.

B. Time-Domain Analysis

Consider the section of N-coupled nonuniform transmission lines shown in Fig. 2(b). Such structures arise frequently in high-speed digital circuits where bus lines have to be deformed to meet spatial constraints imposed by chip sizes and pin-to-pin spacing. In this case, the interest is in the transient response of the structure to various combinations of excitation pulses and arbitrary terminating loads at its ports. This transient response will be computed based on the time-domain S-parameters resulting from a Fourier transform of the corresponding frequency-domain data, which, in turn, are computed using the above-described technique. While a general approach can be developed for this purpose, it is much more efficient to consider the two types of terminating loads, namely, the linear and nonlinear, separately. The following sections present the detailed formulation for the transient analysis of each of these two cases.

1) Linear Terminations: When dealing with linear loads, it is possible to do much of the work in the frequency domain since their frequency-domain impedances are readily available. For this reason, we start by finding a frequency-domain representation of the transient excitation signal. This is a relatively easy task since, in most cases, the Fourier transformation $E(\omega)$ of the transient voltage source $e(t)$ can be calculated analytically. For example, the frequency representation $E(\omega)$ of a pulse with

amplitude e_0, delay time t_d, rise time t_r, fall time t_f, and width t_w is given by

$$E(\omega)=\frac{e_0}{\omega^2}\left[\frac{e^{-j\omega t_d}}{t_r}\left(e^{-j\omega t_r}-1\right)-\frac{e^{-j\omega(t_r+t_w)}}{t_f}\left(e^{-j\omega t_f}-1\right)\right] \quad (16)$$

for $\omega > 0$ and $E(0)=(e_0/4)(t_r+2t_w+t_f)$. Referring to Fig. 2(a) and denoting the incident waves vector by $\overline{A}(\omega)$ and the reflected waves vector by $\overline{B}(\omega)$, we can write the following equations for the total voltage and current values at the various ports:

$$\overline{V}(\omega)=R_{\rm ref}^{-1/2}\left(Z_{\rm ref}^{*}\overline{A}(\omega)+Z_{\rm ref}\overline{B}(\omega)\right) \quad (17a)$$

$$\overline{I}(\omega)=R_{\rm ref}^{1/2}\left(\overline{A}(\omega)-\overline{B}(\omega)\right) \quad (17b)$$

where $Z_{\rm ref}=\mathrm{diag}(Z_{\rm ref1}, Z_{\rm ref2}, \cdots, Z_{\rm ref2N})$ is the diagonal normalizing impedance matrix used for the S-parameter computation. $Z_{\rm ref}^{*}=\mathrm{conj}(Z_{\rm ref})$ is the complex conjugate of $Z_{\rm ref}$ and $R_{\rm ref}=\mathrm{real}(Z_{\rm ref})$ is the real part of $Z_{\rm ref}$. On the other hand, from the definition of the S-matrix, $\overline{A}(\omega)$ and $\overline{B}(\omega)$ must also satisfy

$$\overline{B}(\omega)=S(\omega)\overline{A}(\omega) \quad (18)$$

where $S(\omega)$ is the frequency-domain S-parameter matrix of the structure. In theory, the only requirement in computing the S-matrix is that all entries of $Z_{\rm ref}$ have positive real parts. This condition will ensure time-domain computational stability. Equations (17) and (18) hold for any passive multiport network. To include the effects of the sources, given by the vector $E(\omega)$, and terminating loads, given by the diagonal matrix $Z(\omega)$, the following additional equation can be obtained using Kirchov's law at the ports:

$$\overline{V}(\omega)=\overline{E}(\omega)-Z(\omega)\overline{I}(\omega). \quad (19)$$

Substituting (17) in (19) gives

$$\overline{A}(\omega)=T(\omega)\overline{E}(\omega)+\Gamma(\omega)\overline{B}(\omega) \quad (20)$$

where

$$T(\omega)=R_{\rm ref}^{1/2}\left(Z(\omega)+Z_{\rm ref}^{*}\right)^{-1} \quad (21a)$$

is a diagonal matrix of transmission coefficients and

$$\Gamma(\omega)=T(\omega)\left(Z(\omega)-Z_{\rm ref}\right)R_{\rm ref}^{-1/2} \quad (21b)$$

is a diagonal matrix of reflection coefficients. Combining (18) and (20) with (17a) and solving for $\overline{V}(\omega)$ gives

$$\overline{V}(\omega)=R_{\rm ref}^{-1/2}\Big(Z_{\rm ref}^{*}+Z_{\rm ref}S(\omega)\Big)\cdot\Big(I_d-\Gamma(\omega)S(\omega)\Big)^{-1}T(\omega)\overline{E}(\omega). \quad (22)$$

The transient response $\overline{V}(t)$ of the multiport structure can now easily be recovered from $\overline{V}(\omega)$ by an inverse Fourier transformation.

2) Nonlinear Terminations: The main problem with nonlinear terminations resides in the difficulty in modeling their frequency-domain behavior. Therefore, we must characterize such loads by their time-varying diagonal impedance matrix $Z(t)$. This matrix is commonly obtained from the nonlinearities' I–V characteristics using a Newton–Raphson. Note that $Z(t)$ is not the Fourier transform of the $Z(\omega)$ used in the linear loads case, but is rather the instantaneous impedance matrix seen at the ports of the structure. It relates the instantaneous voltage, current, and source vectors at the ports by

$$\overline{V}(t)=\overline{E}(t)-Z(t)\overline{I}(t). \quad (23)$$

At the same time, $V(t)$ and $I(t)$ satisfy a relationship similar to that of (20), but at each instant, namely,

$$\overline{V}(t)=Z_{\rm ref}^{1/2}\Big(\overline{A}(t)+\overline{B}(t)\Big) \quad (24a)$$

$$\overline{I}(t)=Z_{\rm ref}^{-1/2}\Big(\overline{A}(t)-\overline{B}(t)\Big) \quad (24b)$$

where the normalizing impedance matrix must be real, i.e., $Z_{\rm ref}=Z_{\rm ref}^{*}=R_{\rm ref}$. Combining (23) with (24), we derive the basic generalized equation relating the instantaneous incident and reflected wave vectors as follows:

$$\overline{A}(t)=T_{\rm inst}(t)\,\overline{E}(t)+\Gamma_{\rm inst}(t)\,\overline{B}(t). \quad (25)$$

Again, note that this equation has the same form as (20), but is not its Fourier-transformed version since it holds at each instant in time. The instantaneous transmission and reflection coefficient diagonal matrices $T_{\rm inst}(t)$ and $\Gamma_{\rm inst}(t)$ are found to be

$$T_{\rm inst}(t)=Z_{\rm ref}^{1/2}\Big(Z(t)+Z_{\rm ref}\Big)^{-1} \quad (26a)$$

$$\Gamma_{\rm inst}(t)=T_{\rm inst}(t)\Big(Z(t)-Z_{\rm ref}\Big)Z_{\rm ref}^{-1/2}. \quad (26b)$$

To solve for $V(t)$ and, subsequently $I(t)$, an additional relationship between $\overline{A}(t)$ and $\overline{B}(t)$ is needed. Here we can make use of the frequency-domain characterization of the nonuniform coupled-line structure by writing the time-domain equivalent to (18), namely,

$$\overline{B}(t)=S(t)*\overline{A}(t) \quad (27)$$

where $*$ denotes the convolution product defined in discrete form by

$$X(q)*Y(q)=\sum_{p=0}^{q}X(p)Y(q-p)\Delta\tau. \quad (28)$$

Using this numerical form of the convolution, (27) becomes

$$\overline{B}(t)=S(0)\Delta\tau\overline{A}(t)+\overline{M}(t) \quad (29)$$

where $\overline{M}(t)$ is a $2N$ quasi-independent voltage source vector considered as a memory term containing the history of the network up to time $(\xi-1)$, and is given by

$$\overline{M}(\xi)=\sum_{p=0}^{\xi-1}S(\xi-p)\overline{A}(p)\Delta\tau \quad (30)$$

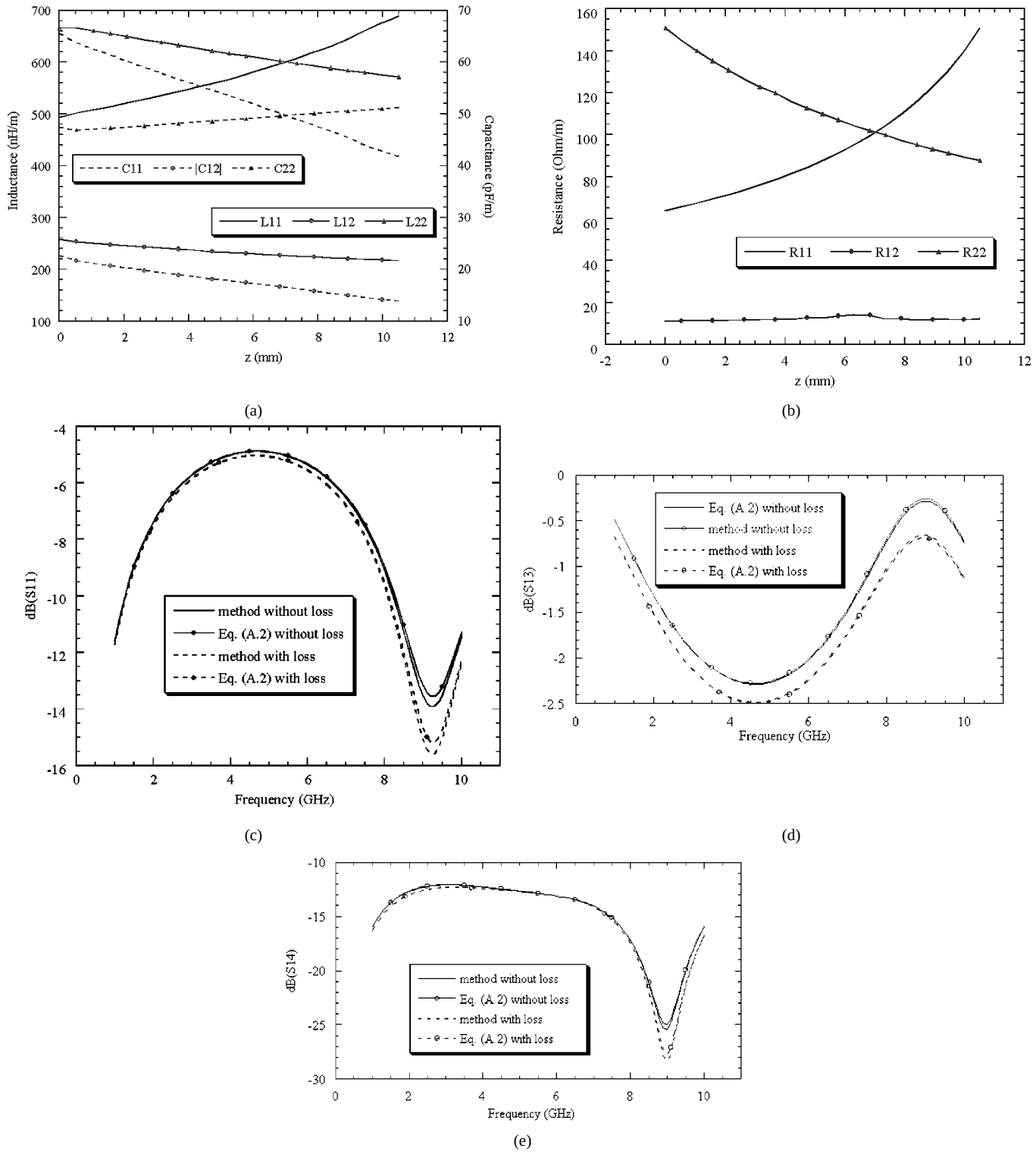

Fig. 6. Analysis of the asymmetric coupled microstrip lines of Fig. 5. (a) z-dependent entries of the inductance and capacitance matrices per unit length. (b) z-dependent entries of the resistance matrix per unit length. (c) Reflection coefficient at port 1: S_{11}. (d) Transmission coefficient between ports 3–1: S_{13}. (e) Isolation coefficient between ports 4–1: S_{14}.

where $\Delta\tau$ is the time step chosen for the simulation and ξ is the normalized time variable given by $\xi = t/\Delta\tau$. Next, combining (25) and (30), the following expression for $\overline{A}(t)$ is derived:

$$\overline{A}(t) = (I_d - \Gamma_{\text{inst}}(t)S_0)^{-1}\left(T_{\text{inst}}(t)\overline{E}(t) + \Gamma_{\text{inst}}(t)\overline{M}(t)\right) \tag{31}$$

where the term S_0 is given by $S_0 = S(0)\Delta\tau$. With $\overline{A}(t)$ and $\overline{B}(t)$ given by (31) and (29), respectively, the instantaneous voltage and current vectors are directly computed using (24).

3) Features of the Proposed Approach: The above formulation offers the following advantages.

- Since the S-parameters used in our approach are generalized (i.e., not modal), any passive multiport network can

be easily incorporated in the time-domain simulation. This is particularly useful for modeling discontinuities, nonuniformity, and any configuration where a modal analysis is not possible. In fact, this technique could be used to simulate the function of a time-domain reflectometer (TDR) that can be coupled to full-wave frequency-domain field solvers in order to locate discontinuities and help optimize transition designs. Furthermore, by using standard S-parameter cascading techniques, complicated networks can be modeled by a single equivalent multiport network and analyzed efficiently in the time domain.

- The fact that the S-parameters can be computed under an arbitrary reference system $Z_{\rm ref}$ gives us added flexibility in the types of passive networks that can be analyzed. More specifically, although most S-parameter calculations are carried out in a fixed 50-Ω reference system, we can easily incorporate S-parameters under other arbitrary normalization systems by using the following renormalization formulas. Let $Z_a = \mathrm{diag}(Z_{a1}, Z_{a2}, \cdots, Z_{aN})$ be an arbitrary diagonal normalizing impedance matrix with $R_a = \mathrm{Real}(Z_a)$ and $Z_a^* = \mathrm{conj}(Z_a)$. Suppose that we have a set of S-parameters in this reference system, i.e., $S(\omega, Z_a)$, and let $Z_{\rm ref} = \mathrm{diag}(Z_{\rm ref1}, Z_{\rm ref2}, \cdots, Z_{refN})$ be the diagonal impedance matrix of the desired new reference system with $R_{\rm ref} = \mathrm{real}(Z_{\rm ref})$ and $Z_{\rm ref}^* = \mathrm{conj}(Z_{\rm ref})$. Through matrix manipulations, one can show that the S-matrix in this new reference system $S(\omega, Z_{\rm ref})$ as a function of that in the original reference system $S(\omega, Z_a)$ is given by

$$S(\omega, Z_{\rm ref}) = R_{\rm ref}^{1/2} (\Psi + Z_{\rm ref})^{-1} (\Psi - Z_{\rm ref}^*) R_{\rm ref}^{-1/2} \quad (32)$$

where

$$\Psi = R_a^{-1/2} (Z_a^* + Z_a S(\omega, Z_a)) (I_d - S(\omega, Z_a))^{-1} R_a^{1/2} \quad (33)$$

and I_d is the identity matrix of order N.

- In light of the above discussion, a particular case of interest is the incorporation of measured S-parameters of a passive multiport circuit in a transient analysis involving the circuit. The approach provides, therefore, a good interface between the time-domain algorithm and measured data.

III. Results

Several nonuniform structures were analyzed in both the frequency and time domains. The results of the frequency-domain analysis are given in terms of the scattering parameters and are grouped in Section III-A. The results of transient analysis are given in terms of the voltage waveforms at the various ports of each structure considered and are presented in Section III-B.

A. Frequency-Domain Results

To illustrate the accuracy and efficiency of the proposed approach for the S-parameter calculation, several nonuniform structures were analyzed. A detailed discussion of the robustness of this technique can be found in [6].

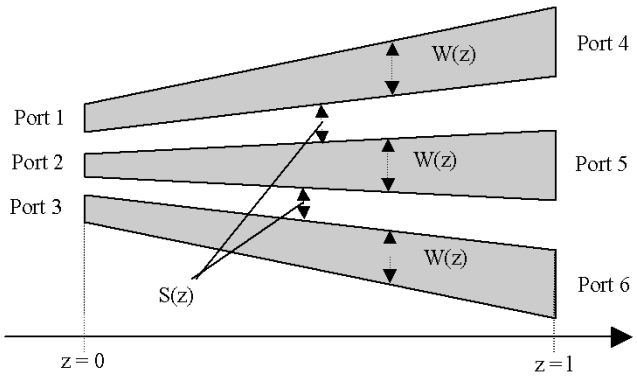

Fig. 7. Geometry of the tapered three-line microstrip structure. $\varepsilon_r = 4.2$, $H = 20$ mil, $W(z) = W_0(1+2z/l)$, $S(z) = 0.5\,W_0(1+z/l)$, $W_0 = 0.24$ mm, and $l = 20$ mm.

1) Tapered Microstrip Line: The first structure is a conventional linear microstrip line taper with the dimensions shown in Fig. 3. This transition has been analyzed by the present approach using two and three basis functions, as well as by a popular commercial circuit simulator.[1] The results obtained are shown in Fig. 4(a) and (b). The rapid convergence of the proposed technique can be seen as excellent agreement with the circuit simulator is obtained over the entire frequency band with only three basis functions. While these results are indicative of the accuracy of the proposed approach, its advantages can be best seen by considering multiple coupled lines.

2) Nonuniform Asymmetric Coupled Microstrip Lines: To best illustrate the ability of the proposed method to handle arbitrary coupled transmission lines, including loss, the asymmetric structure of Fig. 5 is considered. First, the z-dependent $RLGC$ matrices of the structure were computed at 21 z-positions using a 2-D quasi-static finite-element solution at each position.[2] These same parameters were also computed via the more rigorous full-wave solver and were found to have very little dispersion for the $L(z)$, $C(z)$ and $G(z)$ matrices over the frequency range of 0–10 GHz, with $G(z)$ having negligible values. However, conductor losses $R(z)$ were found to be significant and frequency dependent of the form $R = R_0\sqrt{f(\mathrm{GHz})}$, with dominant diagonal terms. The z-dependant inductance and capacitance parameters are shown in Fig. 6(a) while the entries of the symmetric resistance matrix R_0, computed at $f = 1$ GHz, are presented in Fig. 6(b). The structure has then been simulated using the proposed approach and its S-parameters were computed with and without conductor loss included. To validate the results of the proposed approach, the same structure was approximated by 21 cascaded sections of uniform asymmetric coupled lines having different strip widths and spacing. The S-parameters of each uniform section are computed using (A.2) and the overall S-parameters of the nonuniform structure are obtained by simple multiplication of the corresponding T matrices. The magnitude of S_{11}, S_{13}, and S_{14} for both lossy and lossless cases,

[1]HP Microwave Design System (MDS), Building and Analyzing Circuits, Hewlett-Packard, Santa Rosa, CA 1990.

[2]High Frequency Integrated Simulator (HIFIS), Integrated Microwave Technologies Inc., Montréal, P.Q., Canada, 1997.

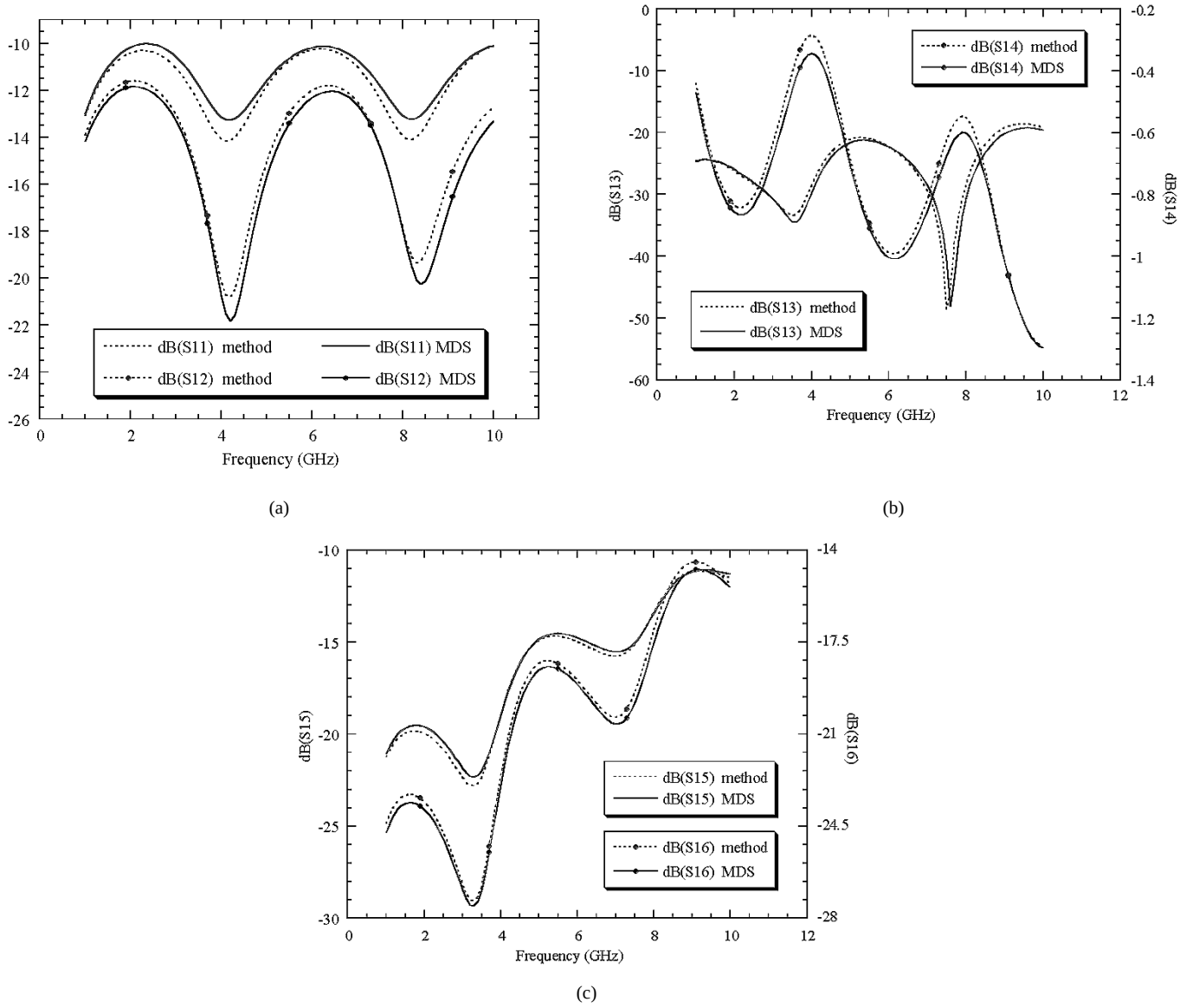

Fig. 8. Frequency-domain analysis of a nonuniform three-coupled line structure. (a) Magnitude of S_{11} and S_{12}. (b) Magnitude of S_{13} and S_{14}. (c) Magnitude of S_{15} and S_{16}.

and using the proposed approach as well as the cascading technique, are shown in Fig. 6(c)–(e). Good agreement between the two sets of results is observed.

3) Three Nonuniform Coupled Microstrip Lines: To further illustrate the advantages of the proposed approach, consider the three-line structure shown in Fig. 7. The choice of this structure is motivated by the need to compare our results with those of circuit simulator having a built-in model for uniform three coupled lines. To analyze this structure, we first computed the values of the 3×3 L and C matrices at ten equidistant points along the z-axis using a finite-element approach. Using these line parameters, the structure was simulated between 1–10 GHz. The same structure was approximated in the circuit simulator by ten cascaded sections of uniform three coupled microstrip lines and analyzed over the same frequency range. Fig. 8(a)–(c) show various S-matrix entries versus frequency as obtained by our approach and those of the circuit simulator. Good agreement between both simulations is seen. It should be noted that only five basis functions were used in this simulation.

4) Nonuniform Ultrawide-Band Directional Coupler: Since the proposed approach is both efficient and accurate, it can easily be used to optimize the design of nonuniform line couplers, filters, and matching circuits based on nonuniform lines. To illustrate this, we consider a nonuniform directional coupler whose performance is given in terms of its electrical parameters, namely, coupling profile, characteristic impedance, phase velocity, and electrical length. The synthesis of such couplers can be done using the technique described in [7]. The particular coupler considered here is a 50-Ω 14-dB coupler covering the frequency range of 3–20 GHz. Using a phase velocity of 0.98×10^8 m/s the coupling profile, i.e., the coupling factor as a function of position, $k(z)$ and the length l were determined. Given the coupling factor at each position

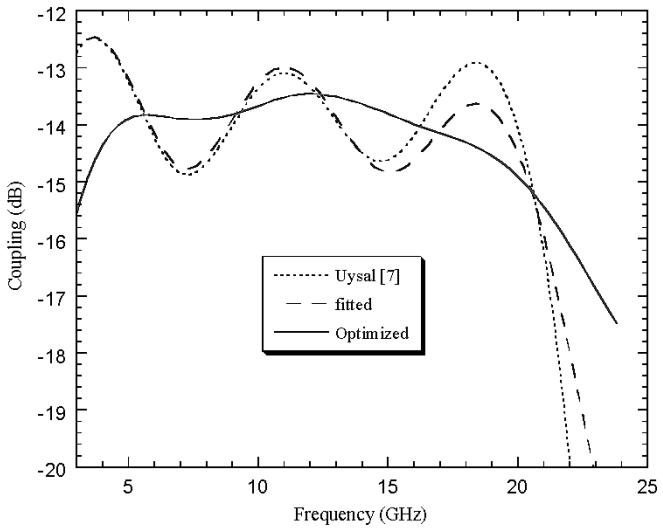

(a)

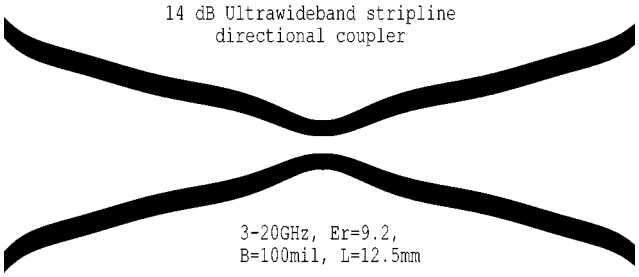

(b)

Fig. 9. Ultrawide-band 14-dB 3–20-GHz directional coupler in edge-coupled striplines. (a) Simulated coupling coefficient. (b) Layout of the optimized coupler.

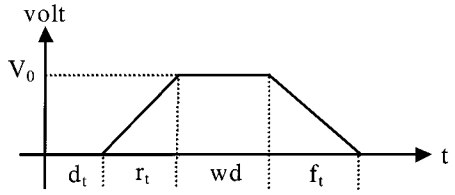

Fig. 10. General description of the excitation pulses used in the transient simulations.

and a constant 50-Ω characteristic impedance, the 2×2 L and C matrices are computed as follows:

$$L = \begin{bmatrix} L_0 & L_m \\ L_m & L_0 \end{bmatrix} \quad \text{and} \quad C = \begin{bmatrix} C_0 & C_m \\ C_m & C_0 \end{bmatrix}$$

where

$$L_0(z) = \frac{\sqrt{\varepsilon_r}}{2c}\left(Z_e(z) + Z_o(z)\right)$$
$$L_m(z) = \frac{\sqrt{\varepsilon_r}}{2c}\left(Z_e(z) - Z_o(z)\right)$$
$$C_0(z) = \frac{\sqrt{\varepsilon_r}}{2c}\left(\frac{1}{Z_e(z)} + \frac{1}{Z_o(z)}\right)$$

and

$$C_m(z) = \frac{\sqrt{\varepsilon_r}}{2c}\left(\frac{1}{Z_e(z)} - \frac{1}{Z_o(z)}\right)$$

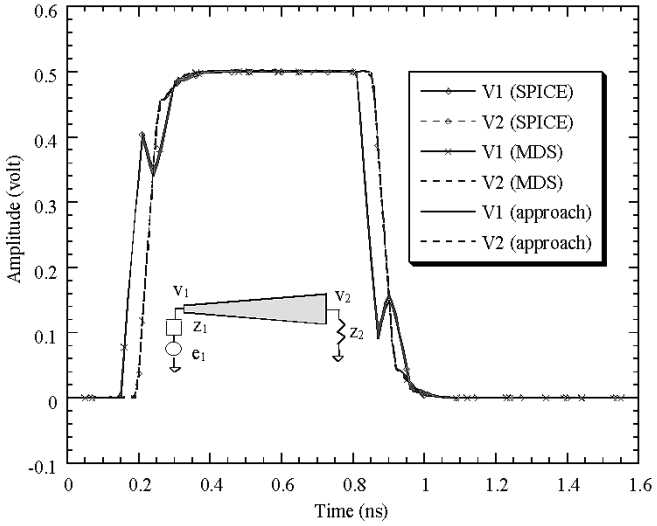

(a)

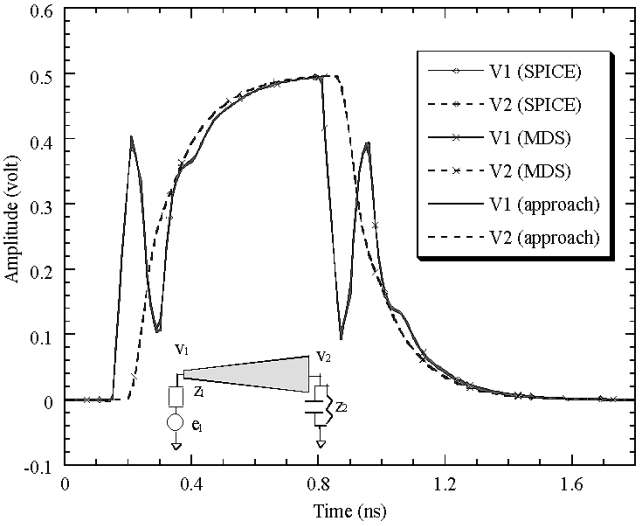

(b)

Fig. 11. Transient analysis of a linear microstrip taper under: (a) resistive and (b) reactive terminations.

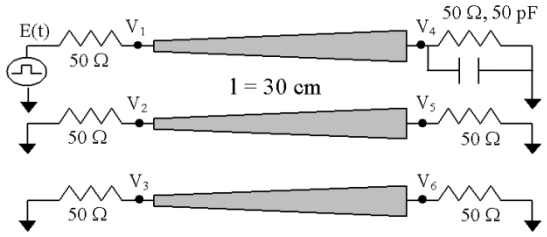

Fig. 12. Configuration of a nonuniform three-line structure terminated by reactive loads.

where

$$Z_e(z) = Z_0\sqrt{\frac{1+K(z)}{1-K(z)}} \quad \text{and} \quad Z_o(z) = Z_0\sqrt{\frac{1-K(z)}{1+K(z)}}$$

$Z_0 = 50\ \Omega$ and c is the velocity of light in the vacuum. Once L and C are calculated, the present approach is used to compute

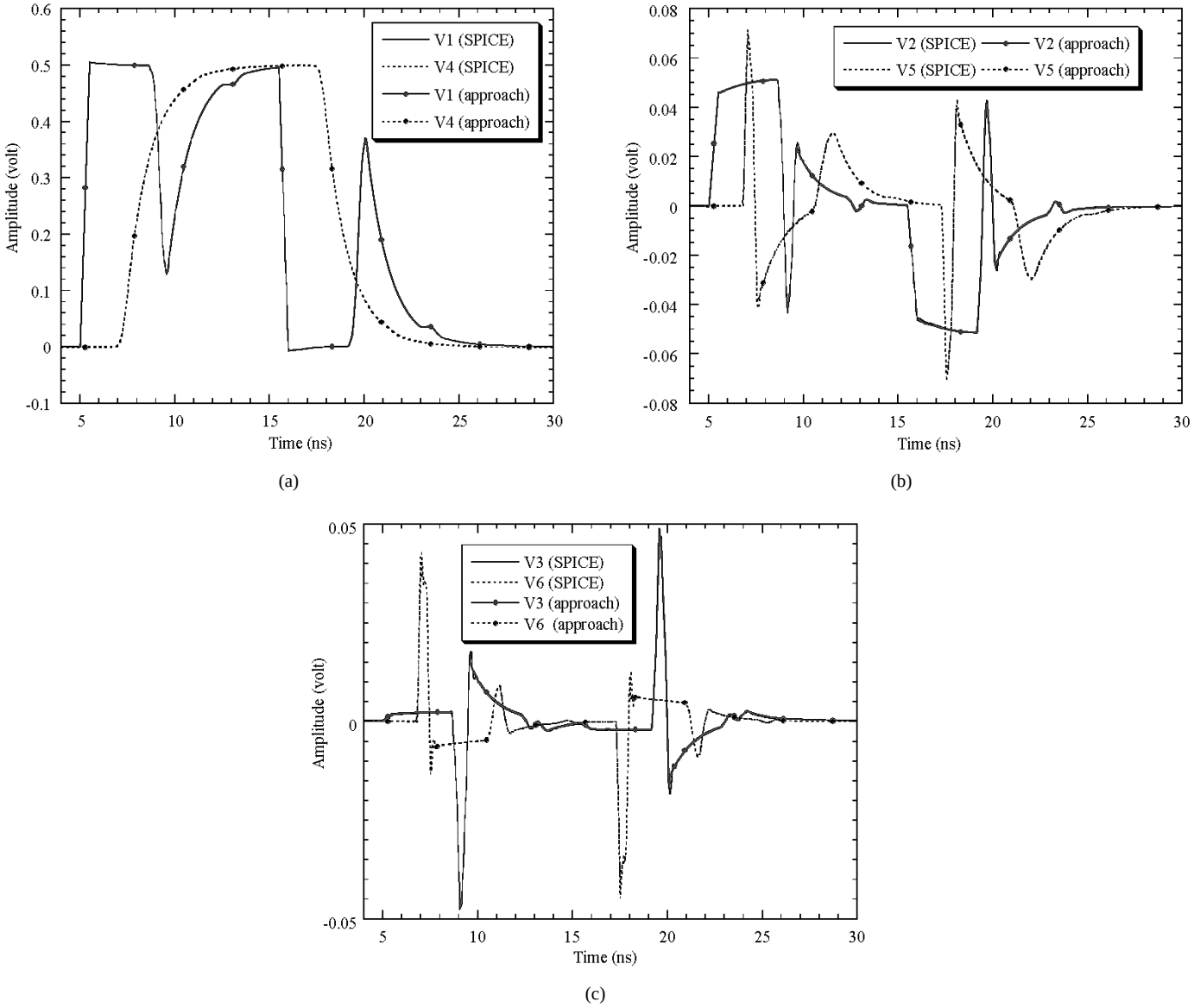

Fig. 13. Transient analysis of the configuration of Fig. 12. (a) Response at nodes 1 and 4: near and far ends of the driven line. (b) Response at nodes 2 and 5: crosstalk on middle line. (c) Response at nodes 3 and 6: crosstalk on the far line.

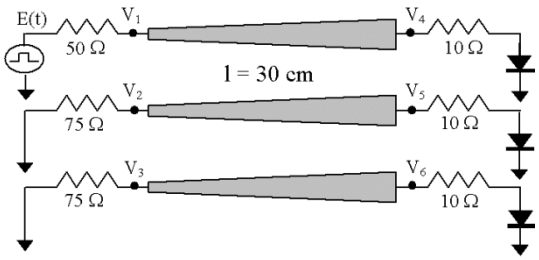

Fig. 14. Configuration of a nonuniform three-line structure terminated by nonlinear loads (diodes).

the coupling factor as a function of frequency $C(\omega)$. Fig. 9(a) shows the results of this analysis as the curve labeled "Uysal" [7]. It can be seen from this curve that the ripple in the coupling coefficient is as high as ± 1.5 dB. To optimize this performance, the coupling profile $K(z)$ must be represented by a polynomial whose parameters can be subsequently adjusted until the desired frequency response $C_d(\omega)$ is obtained. The curve labeled "fitted" in Fig. 9(a) shows the coupling obtained as a result of a polynomial fitting of $K(z)$. Note that given the limited accuracy of this fitting, the resulting coupling deviates slightly from the original form. By manually adjusting few coefficients in the fitting polynomial, the performance of the coupler can be improved substantially, as shown by the curve labeled "optimized" in Fig. 9(a). The layout of this optimized coupler, implemented in edge-coupled stripline, is shown in Fig. 9(b). Clearly, further improvements can be achieved if the entire optimization procedure is automated and driven by a good optimization algorithm.

B. Time-Domain Results

To validate the proposed approach for transient response calculation, coupled- and single-line structures were analyzed under different excitations and linear and nonlinear terminations. The excitations are all in the form of pulses that are described by a delay time d_t, rise time r_t, fall time f_t,

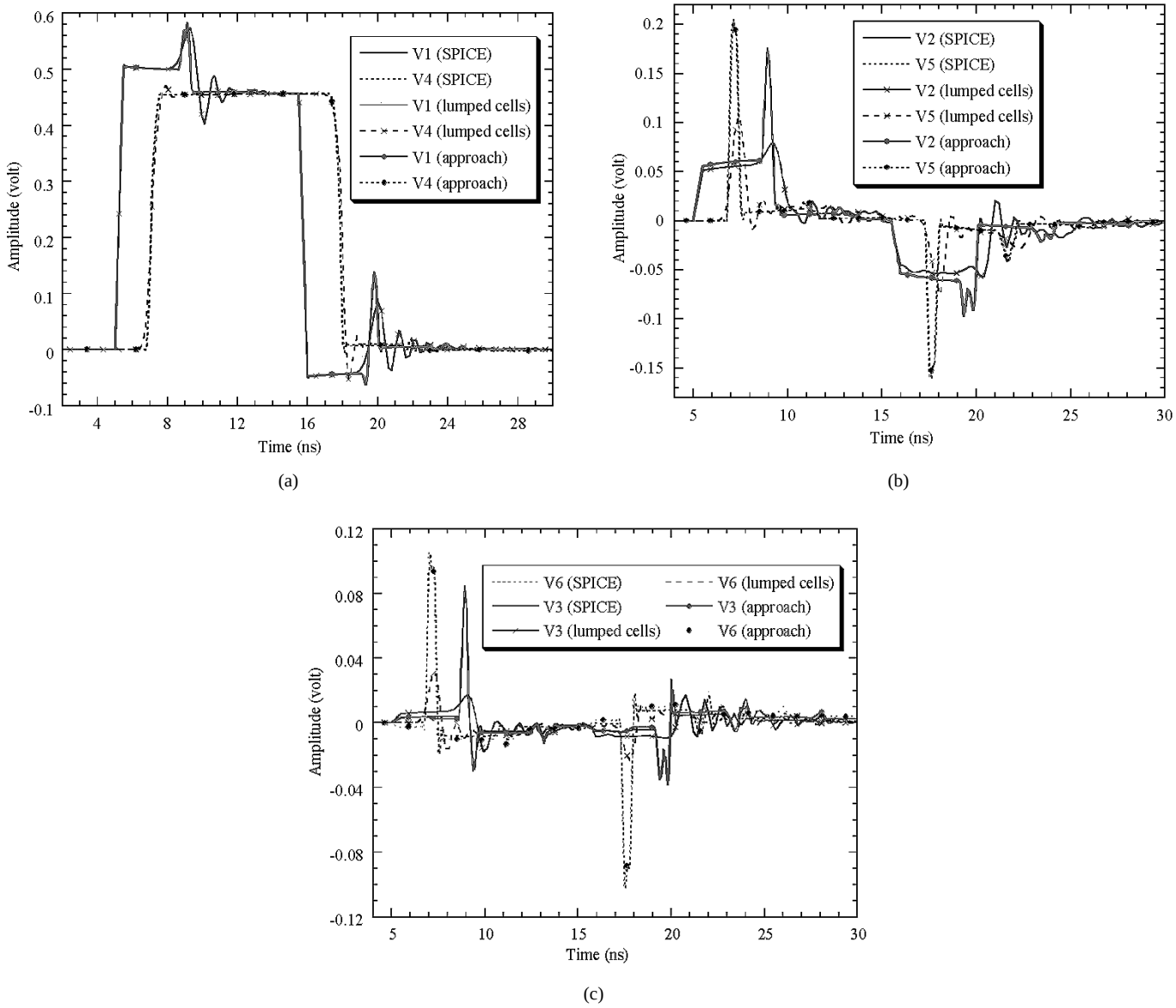

Fig. 15. Transient analysis of the configuration of Fig. 14. (a) Response at nodes 1 and 4: near and far ends of the driven line. (b) Response at nodes 2 and 5: crosstalk on middle line. (c) Response at nodes 3 and 6: crosstalk on the far line.

duration or width w_d, and an amplitude V_o, as shown in Fig. 10. All results are compared to those obtained by a commercial time-domain CAD program.

1) Tapered Microstrip Line: This structure is the same as the one analyzed in Section III-A and shown in Fig. 3. The taper is excited at the port 1 by a pulse having d_t = 150 ps, r_t = 60 ps, f_t = 60 ps, w_d = 0.6 ns, and V_o = 1 V. The simulation duration is set to 1.7 ns with a time step of 10 ps. First, the structure is terminated by resistive loads at both ends ($Z_1 = Z_2 = 50\ \Omega$) and analyzed by our approach as well as by SPICE, using ten cascaded uniform transmission-line sections, and MDS, using its built-in taper model. The results of these analyses are summarized in Fig. 11(a) and show that all three solutions are virtually identical. Fig. 11(b) shows similar results, but with the structure terminated by a reactive load at the second port ($Z_2 = 50\ \Omega//4$ pF). Again, good agreement between the solutions is observed.

2) Three Coupled Lines with Arbitrary Loads: To further validate the proposed transient analysis method and its flexibility, we consider an arbitrary three-line structure with the following position dependent L and C matrices [9]:

$$L = \begin{bmatrix} L_0 & L_m & 0 \\ L_m & L_0 & L_m \\ 0 & L_m & L_0 \end{bmatrix} \quad C = \begin{bmatrix} C_0 & C_m & 0 \\ C_m & C_0 & C_m \\ 0 & C_m & C_0 \end{bmatrix}$$

where

$$\begin{aligned} L_0(z) &= l_0\,(1 + k_1(z)) \\ L_m(z) &= k_1(z) L_0(z) \\ k_1 &= 0.1\left(1 + 0.6\sin\left(\pi z + \pi/4\right)\right) \\ l_0 &= 387\ \text{nH/m} \\ C_0(z) &= c_0/\left(1 - k_2(z)\right) \\ C_m(z) &= -k_2(z) C_0(z) \\ k_2(z) &= 0.15\left(1 + 0.6\sin\left(\pi z + \pi/4\right)\right) \\ c_0 &= 104.13\ \text{pF/m} \end{aligned}$$

$$\begin{bmatrix} E^{-1}+Z_{\rm ref}^{0}H^{-1}Z_m^{-1} & E^{-1}-Z_{\rm ref}^{0}H^{-1}Z_m^{-1} \\ \left(E^{-1}-Z_{\rm ref}^{l}H^{-1}Z_m^{-1}\right)W(-l) & \left(E^{-1}+Z_{\rm ref}^{l}H^{-1}Z_m^{-1}\right)W(l) \end{bmatrix} \begin{bmatrix} \overline{A} \\ \overline{B} \end{bmatrix} = \begin{bmatrix} \mathrm{diag}(\overline{E}_0) & 0_N \\ 0_N & \mathrm{diag}(\overline{E}_l) \end{bmatrix} \tag{A.2}$$

$$R_m = R_0 = G_0 = G_m = 0.$$

Fig. 12 shows the configuration of the three-line structure with linear terminating loads at all ports. The first line of this structure is excited by a pulse described by $d_t = 5$ ns, $r_t = 0.5$ ns, $f_t = 0.5$ ns, $w_d = 10$ ns, and $V_o = 1$ V. The results of this simulation are shown in Fig. 13(a)–(c) and include a comparison with a SPICE simulation using 40 cascaded uniform coupled three-line sections. The SPICE representation of each of these sections is based on the modal decomposition described in [10]. It should be noted that agreement seen in these figures could not be achieved until such a high number of sections were used in SPICE.

Fig. 14 shows the same three-line structure, but terminated with three nonlinear loads. The structure is excited in a similar fashion to the linear termination case, and the results of the analysis are shown in Fig. 15(a)–(c). These figures also show the transient responses obtained by using two different SPICE models. The first model is based on cascading 40 uniform sections, the minimum required for conversion, as described above. The second model is based on cascading 40 cells of lumped-element networks representing the self and mutual terms by lumped inductance and capacitance elements. It is seen from the results that while both our approach and the first SPICE model give comparable results, the second SPICE model fails to converge to these results even when the number of cells is increased.

It should be noted that in the above analyses, the lines were assumed to be lossless because of the limitation in the SPICE models. However, our approach can easily account for conductor or dielectric losses in arbitrary nonuniform structures.

IV. Conclusion

New formulations for the frequency- and time-domain analysis of multiple coupled nonuniform lines have been presented in this paper. The frequency-domain analysis uses new frequency-dependent basis function in a robust method-of-moment approach yielding accurate results over large frequency ranges. Using only a moderate number of basis functions, illustrative examples of single, coupled, and three-line structures were successfully analyzed. The efficiency of the approach was further demonstrated by optimizing the performance of an ultrawide-band coupler with very little effort. The time-domain approach uses the structure's S-parameters in the frequency domain, when only linear terminations are present, or in the time domain, when nonlinear loads are used, and the terminating source and load conditions to obtain its transient response. Since the S-parameters used account for dielectric and conductor losses in the passive structure, these effects are automatically accounted for in the structure's transient response. Results for multiple coupled lines showing various signal distortion effects, i.e., delay, crosstalk, reflection, etc., have been presented and compared to SPICE. Several advantages and features of the current approach have also been highlighted.

Appendix
Derivation of the Generalized S-Parameters for Uniform Coupled Lines

In the case of uniform coupled lines, an analytic solution for their S-parameters can be obtained. In [8], a method for calculating the modal S-parameters has been presented. This method assumes that the structure is excited by modal voltages and currents and is terminated by modal matching impedances. Based on this method, and using a simplified version of the current technique, one can derive the generalized line S-parameters of uniform coupled lines. For this purpose, (15) can still be used, except that the port voltages V_{mn} are now simply deduced from the following equation:

$$\overline{V}(f, z) = E^{-1}\Big(W(-z)\overline{A} + W(z)\overline{B}\Big) \tag{A.1}$$

where $\overline{A}$ and $\overline{B}$ are two voltage vectors associated with the incident and reflected waves, respectively. It can easily be shown that these vectors satisfy the system of equations, shown in (A.2), at the top of this page, where $W(z) = \mathrm{diag}(e^{\gamma_1 z}, e^{\gamma_2 z}, \cdots e^{\gamma_N z})$, $Z_m = (\mathrm{diag}(\overline{\gamma}))^{-1}EZH^{-1}$, and E and H are as defined in (5). Using the solution of (A.2) under different excitation for the vectors A and B in (A.1) and substituting the resulting V_{nm} expression in (15), the generalized line S-parameters of the uniform coupled lines are obtained.

Acknowledgment

The authors would like to thank the reviewers for their helpful comments and suggestions.

References

[1] M. A. Mehalic and R. Mittra, "Investigation of tapered multiple microstrip lines for VLSI circuits," *IEEE Trans. Microwave Theory Tech.*, vol. 38, pp. 1559–1567, Nov. 1990.

[2] G. Pan, G. J. Wunsch, and B. K. Gilbert, "Frequency-domain analysis of coupled nonuniform transmission lines using Chebychev pseudo-spatial techniques," *IEEE Trans. Microwave Theory Tech.*, vol. 40, pp. 2025–2033, Nov. 1992.

[3] O. A. Palusinski and A. Lee, "Analysis of transients in nonuniform and uniform multiconductor transmission lines," *IEEE Trans. Microwave Theory Tech.*, vol. 37, pp. 127–138, Jan. 1989.

[4] A. B. Kouki, A. Hamade, and F. M. Ghannouchi, "A new formulation for the analysis of nonuniform transmission lines using frequency-varying basis functions," in *IEEE MTT-S Int. Microwave Symp. Dig.*, Orlando, FL, May 1995, pp. 817–820.

[5] N. Boulejfen, A. B. Kouki, and F. M. Ghannouchi, "Transient analysis of high speed digital interconnects with nonuniform coupled lines," *Microwave Opt. Technol. Lett.*, vol. 11, no. 6, pp. 308–313, Apr. 1995.

[6] ——, "A robust and efficient method for the frequency domain analysis of nonuniform, lossy multi-line transmission structures," in *IEEE MTT-S Int. Microwave Symp. Dig.*, Baltimore, MD, July 1998, pp. 1763–1766.

[7] S. Uysal, *Nonuniform Line Microstrip Directional Couplers and Filters*. Norwood, MA: Artech House, 1993.

[8] J. E. Schutt-Aine and R. Mittra, "Nonlinear transient analysis of coupled transmission lines," in *IEEE Trans. Microwave Theory Tech.*, vol. 36, Mar. 1988, pp. 529–535.
[9] J. Mao and Z. Li, "Analysis of the time response of multiconductor transmission lines with frequency-dependent losses by convolution-characteristics," *IEEE Trans. Microwave Theory Tech.*, vol. 40, pp. 637–644, Apr. 1992.
[10] C. Paul, *Electromagnetic Compatibility*. Norwood, MA: Artech House, 1992.

Noureddine Boulejfen was born in Kairouan, Tunisia, on February 22, 1968. He received the electrical engineering degree from the Ecole Nationale des Ingénieurs de Monastir, Monastir, Tunisia, in 1993, and the M.Sc.A. degree from the Ecole Polytechnique de Montréal, Montréal, P.Q., Canada, in 1996, and is currently working toward the Ph.D. degree at Ecole Polytechnique de Montréal.

He is currently a Research Associate with the Microwave and Space Electronics Group (Poly-Grames), Ecole Polytechnique de Montréal. His main interests are in the area of applied numerical techniques for the modeling of wide-band microwave structures and high-speed digital interconnects. He has also worked extensively on the development of multiport, frequency and time-domain measurement systems.

Ammar B. Kouki (S'88–M'92) was born in Teboursouk, Tunisia. He received the B.S. and M.S. degrees in engineering science from Pennsylvania State University, University Park, in 1985 and 1987, respectively, and the Ph.D. degree in electrical engineering from the University of Illinois at Urbana-Champaign, in 1991.

He is currently an Associate Professor in the Electrical Engineering Department, Ecole de Technologie Superieure, Montréal, P.Q., Canada. His main research interests are in the areas of numerical techniques for passive structure modeling and design, active device modeling and characterization, and the development of innovative educational tools for teaching microwave courses.

Fadhel M. Ghannouchi (S'84–M'88–SM'93) received the degree in physics/chemistry from the University of Tunis, Tunis, Tunisia, in 1980, the B.Eng. degree in engineering physics, and the M.S. and Ph.D. degrees in electrical engineering from the Ecole Polytechnique de Montréal, Montréal, P.Q., Canada, in 1983, 1984, and 1987, respectively.

He is currently a Professor with the Electrical Engineering Department, Ecole Polytechnique de Montréal, where, since 1984, he has been teaching electromagnetics and microwave theory and techniques. His research interests are in the areas of microwave/millimeter-wave instrumentation and measurements, nonlinear modeling of microwave active devices, and design of power- and spectrum-efficient microwave amplification systems. He is the founder and President of AmpliX Inc., a company that offers linearization products and services to wireless and satcom equipment manufacturers. He has also served on the technical committees of several international conferences and symposiums and provides consulting services to a number of microwave companies.

Dr. Ghannouchi is a Registered Professional Engineer in the Province of Quebec, Canada. He is on the Editorial Board of the IEEE TRANSACTIONS ON MICROWAVE THEORY AND TECHNIQUES.